

Stoner factors of doped 122 Fe-based superconductors: First principles results

Smritijit Sen^{1,2}, Haranath Ghosh^{1,2}

¹*Homi Bhabha National Institute, Anushaktinagar, Mumbai 400 094, India.*

²*Human Resources Development Section, Raja Ramanna Centre for Advanced Technology, Indore -452013, India.*

A comprehensive study on the evolution of Stoner factor with doping concentration for various doped 122 systems (like BaFe₂As₂, SrFe₂As₂) of Fe-based superconductors is presented. Our first principles electronic structure calculations reveal that for Co/Ru (electron or iso-electronic) doping at Fe sites or P doping at As sites result in a reduction of Stoner factor with increasing doping concentration. On the contrary, in case of Na/K (hole) doping at the Ba sites, Stoner factor is enhanced for higher doping concentrations. This may be considered as an indicator of elevation of “magnetic fluctuation” in these systems. We find that the Stoner factor uniquely follows the variation of the pnictide height z_{As} /Fe-As bond length with various kinds of doping. Our calculated Fermi surfaces explicate the diversities in the behaviour of Stoner factors for various doped 122 systems ; larger degree of Fermi surface nesting, larger the value of Stoner factor and vice versa.

I. INTRODUCTION

Invention of superconductivity in Fe-based compounds not only introduced a drastic change in the belief that Fe is inimical to superconductivity due to the presence of strong local magnetic moment associated with Fe atom but also recreate a glimpse of hope for developing a complete generalized theory of high temperature superconductivity. One of the most interesting aspects of these Fe-based superconductors (SCs) from a fundamental point of view, is that superconductivity may arise from magnetic fluctuation or orbital fluctuation [1–5]. However, the glue to the electron-electron attraction or more precisely pairing mechanism in these Fe-based SCs is far from being settled [5–8]. Phase diagrams of Fe-based SCs establish the manifestation of various exotic phases like spin density wave (SDW), orbital order, nematic order, structural transition *etc.* [9–16]. Various physical properties including superconductivity of these Fe-based SCs are very much sensitive to temperature, pressure as well as doping concentration as evident from phase diagrams [17–20]. Influence of structural parameters on the superconducting as well as on other exotic phases is well established through extensive theoretical and experimental investigations [20–22]. Magnetic (antiferromagnetic spin) fluctuation in high T_c cuprates provide pairing in $d_{x^2-y^2}$ channel whereas in Fe-based superconductors it is believed to provide s^\pm pairing symmetry [6]. The quantity that may be used as an indicator of magnetic fluctuation in metallic systems, is Stoner factor. Although Stoner theory is formulated for ferromagnetic instability, it can also be applied for anti-ferromagnetic systems [23].

Broadly, there exists about six invented families of Fe-based SCs [1]. Among all these families 122 family is the most studied one both theoretically and experimentally largely because of availability of high quality single crystals in this family. The generalized chemical formula of 122 family is MFe₂X₂, where M=Ba, K, Ca, Sr and X=As, P. The phase diagrams of 122 family exhibit a

large number of diversities in the physical properties [1]. For example, superconductivity emerges in the electron doped systems (*e.g.*, replacing Co by Fe) with a very small doping concentration ($\sim 2\%$) [13–15] whereas the same arises in hole doped systems with higher doping concentration ($\sim 25\%$) [9]. On the other hand, for the case of iso-electronic Ru doping at the Fe site, superconductivity appears at about 50% Ru doping concentration [24, 25] which is quite high compared to other doped 122 systems. Another qualitatively distinct diversity in the phase diagram of 122 system is observed in case of Na doped Ba122 system [26]. Avci *et al.*, displayed the appearance of an additional C₄ (tetragonal) phase well inside the orthorhombic phase in Ba_{1-x}Na_xFe₂As₂ system at the boundary between superconductivity and SDW (stripe antiferromagnetism) which is different from the previous observations of re-entrant tetragonal phase in electron-doped compounds [15] and has many important consequences. The role of various structural parameters specially z_{As} (fractional z co-ordinate of As atom) or anion height (height of the As atom from the Fe plane) in superconductivity, magnetism and structural transition is indispensable [20, 22, 27–31]. However the inter-relationship among superconductivity, magnetic order, nematic order, orbital order and structural transition is under thorough investigations both theoretically as well as experimentally [3, 5, 32–34]. The presence of magnetic fluctuation in these Fe-based systems is probed by magnetic susceptibility (χ). A large number of theoretical and experimental works are available in the literature addressing the role of magnetic fluctuation in superconductivity and other observed physical properties of Fe-based SCs [32, 35]. An important finding of the present work is that the Stoner factor of various 122 material (that may model magnetic fluctuation) varies with doping in the same fashion as that of the pnictide height or z_{As} .

Density functional theory (DFT), in its most simple implementation [the local-(spin)-density-approximation (L(S)DA)] is in principle an exact theory to estimate the ground state properties of any system. It is now well established that LSDA and generalized gradient

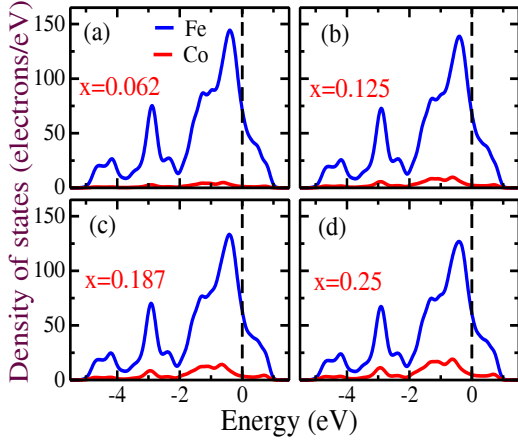


FIG. 1: Calculated atom projected density of states within super-cell method for Fe and Co atoms in Co doped (electron doping) Ba122 system ($\text{BaFe}_{2-x}\text{Co}_x\text{As}_2$) in the tetragonal phase for various doping concentrations, indicated in the figure.

approximation (GGA) approach, which does not take into account the effect of near-critical fluctuations on the long-range magnetism, fails to predict accurate electronic structures for itinerant magnetic system near quantum critical point. A significant amount of effort has been made to introduce these fluctuations within first principles DFT method [36, 37]. Stoner factor is a parameter which mimic the presence of magnetic instability in a system and can be calculated within LSDA approach as shown in ref [23]. However no thorough comprehensive investigations, either theoretically or experimentally exist as to how Stoner factor is being modified due to various kinds of dopings and temperature. In this paper we present a comprehensive picture of Stoner factor for various 122 Fe-based systems as a function of doping concentration from first principles simulations.

We calculate Stoner factor from first principles study of density of states (DOS) for these 122 compounds as a function of doping concentrations. We have found that Stoner factors get modified qualitatively differently for different kinds of doping. For example, in case of electron doping (Co doping at the Fe site) and iso-valent doping (Ru doping at Fe site as well as P doping at As site), Stoner factor gradually decreases with increasing doping concentration. On the other hand, exactly opposite trend in the behaviour of Stoner factor is observed in case of hole doped systems (K/Na doping at the Ba site). This diversity in the behaviour of Stoner factor is then analysed in the light of calculated nature of the FSs of these systems for various doped cases. The method of calculations, including the evaluation of Stoner factor for various doped systems require magnitude of DOS at the Fermi level which are obtained through detailed first principles simulation and are discussed in the forthcoming theoretical method section. An important speciality

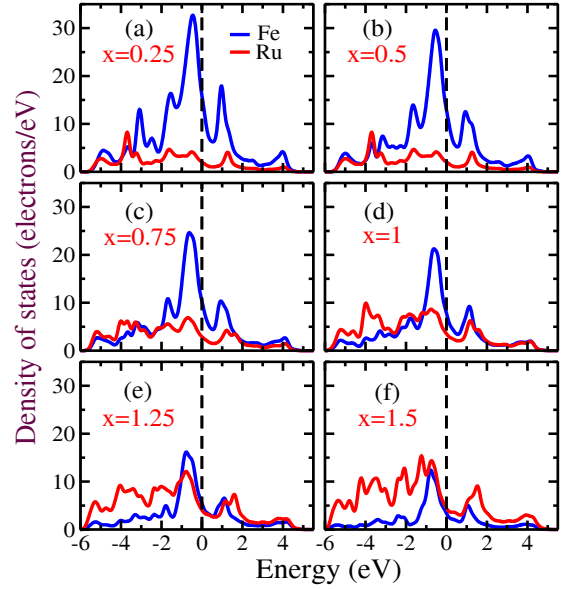


FIG. 2: Calculated atom projected density of states within super-cell method for Fe and Ru atoms in Ru doped (iso-electronic doping) Sr122 system ($\text{SrFe}_{2-x}\text{Ru}_x\text{As}_2$) in the tetragonal phase for various doping concentrations, indicated in the figure.

of our simulation results is that we use exact experimentally determined structural parameters of various doped systems as input which are being kept intact. As a consequence of that, presented results are very much realistic. In the succeeding section we present the variation of Stoner factor with doping concentration for many doped materials of 122 family of Fe-based SCs. Modifications of the FSs are also depicted to elucidate the observed anomalies in the behaviour of Stoner factor with doping. In the last section, we finally conclude and summarize our results.

II. THEORETICAL METHODS

Our first principles electronic structure calculations are performed by implementing ultrasoft pseudopotential with plane wave basis set based on density functional theory [38]. Electronic exchange correlation is treated under the generalised gradient approximation (GGA) using Perdew-Burke-Ernzerhof (PBE) functional [39]. It should be mentioned here that density functional theory within local density approximation (LDA) as well as generalized gradient approximation (GGA) was unable to optimize the experimental value of z_{As} (fractional coordinate of As) with desired accuracy [20, 22, 40–42]. In fact, the optimized value of z_{As} is about 0.1 to 0.15 Å smaller than that of the experimental one. The origin of this discrepancy is the presence of strong magnetic fluctuation, associated with Fe atoms in these materials [43]. Electronic structures (band structure, Fermi

surface *etc.*), calculated using optimized lattice parameters (a , b , c and z_{As}) do not resemble with that of the experimentally measured one [21, 53]. This insist us to employ experimental lattice parameters *i.e.*, a , b , c and z_{As} [9, 13, 19, 22, 44–46] instead of geometry optimized (total energy minimization) lattice parameters as inputs of our first principles electronic structure calculations. We use experimental orthorhombic (low temperature) as well as tetragonal (high temperature) lattice parameters a , b , c and z_{As} as input of our *ab-initio* electronic structure calculations [9, 13, 19, 22, 44–46]. Various modern X-ray diffraction techniques *e.g.*, using Synchrotrons radiation sources *etc.* that determines crystallographic information at different external perturbations (like temperature, chemical doping *etc.*) are essentially result of diffraction from various atomic charge densities (Bragg’s diffraction). Considering experimentally determined structural parameters at different temperatures, doping as input thus in turn provides temperature/doping dependent correct densities to our first principles calculation. These input structural parameters are kept fixed through out the calculation for a fixed doping. This is how we use the DFT formalism to bring out realistic doping dependent observable with the help of experimental input (energy being functional of electron density $E \equiv E[\rho(r, T, x)] \equiv E[\rho(a(x, T), b(x, T), c(x, T))]$. The main effect on the electronic structure from finite temperature/doping is the underlying crystal structure, and the average crystal structure can usually be reliably determined from the diffraction experiment at a given doping.

In order to dope the system, we use two theoretical methods: (1) Virtual crystal approximation (VCA) [47] (2) Super-cell. These two methods are used to prepare various doped Ba122 and Sr122 systems as per requirement. For example, we use super-cell method for calculating the DOS as well as the FSs of Ru doped 122 systems because the VCA method is unable to produce accurate electronic structures in the higher doping regime for these systems. On the contrary, we employed VCA method to dope K, Na and P in Ba122 system. The detailed discussion about the application of VCA and super-cell methods for various doped 122 systems can be found in ref [48]. In this work, we use the VCA method, developed by Bellaiche and Vanderbilt [47] based on weighted averaging of pseudopotentials. It should be noted that although DOS of Co doped 122 systems are calculated using super-cell method, FSs are calculated within VCA method to handle the small percentage of doping in the primitive unit cell. Moreover, size of the super-cells are different for different doping cases. For example, in Ru doped Ba122 and Sr122 systems, we use $\sqrt{2} \times \sqrt{2} \times 1$ super-cells, whereas $2 \times 2 \times 1$ super-cell is used for Co doped 122 materials. Non-spin-polarized and spin polarised single point energy calculations were carried out for tetragonal phase with space group symmetry $I4/mmm$ (No. 139) and orthorhombic phase with space group symmetry $Fmmm$

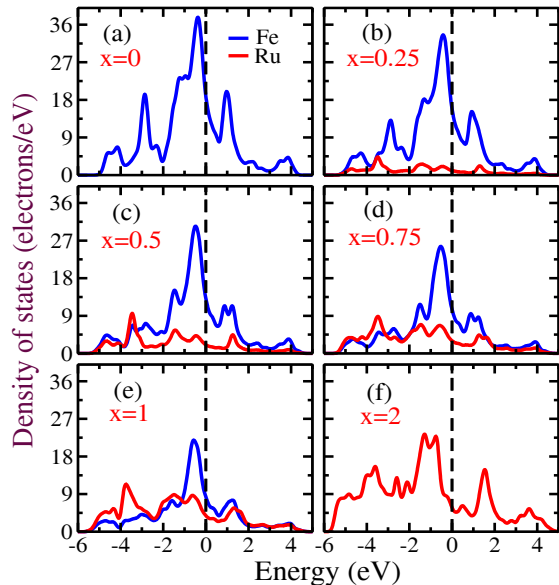


FIG. 3: Calculated atom projected density of states within super-cell method for Fe and Ru atoms in Ru doped (iso-electronic doping) Ba122 system ($BaFe_{2-x}Ru_xAs_2$) in the tetragonal phase for various doping concentrations, indicated in the figure.

(No. 69) respectively using ultrasoft pseudo-potentials and plane-wave basis set with energy cut off 500 eV and higher as well as self-consistent field (SCF) tolerance as 10^{-6} eV/atom. Brillouin zone is sampled in the k space within MonkhorstPack scheme and grid size for SCF calculation is chosen as per requirement of the calculation for various systems and approaches. For simulating Fermi surfaces, grid size of SCF calculation is chosen as $26 \times 26 \times 31$. LDA+U calculations have also been performed for orthorhombic Na and P doped Ba122 systems with SDW spin configuration [49], where doping has been implemented within super-cell method. Stoner factor of a compound like doped 122, can be defined as $I^{Fe} \times [N^{Fe}(E_F)]^2 + I^{Ru/Co} \times [N^{Ru/Co}(E_F)]^2$, where $N^{Fe}(E_F)$ and $N^{Ru/Co}(E_F)$ are the density of states at the Fermi level from Fe and Ru/Co atoms respectively [23, 50]. The values of Stoner parameters I^{Fe} and $I^{Ru/Co}$ are taken from ref [50–52].

III. RESULTS AND DISCUSSIONS

We have studied many doped samples (hole doping, electron doping and iso-valent doping) of 122 Fe-based SCs to study the evolution of Stoner factor with doping concentration. As a representative of hole doped and electron doped systems, we consider Na/K doping (at the Ba site) and Co doping (at the Fe site) of $BaFe_2As_2$ (Ba122) systems respectively. Isovalent or iso-electronic doping at Fe site (Ru doping) for $BaFe_2As_2$ and $SrFe_2As_2$ (Sr122) systems as well as in As site (P doping) for

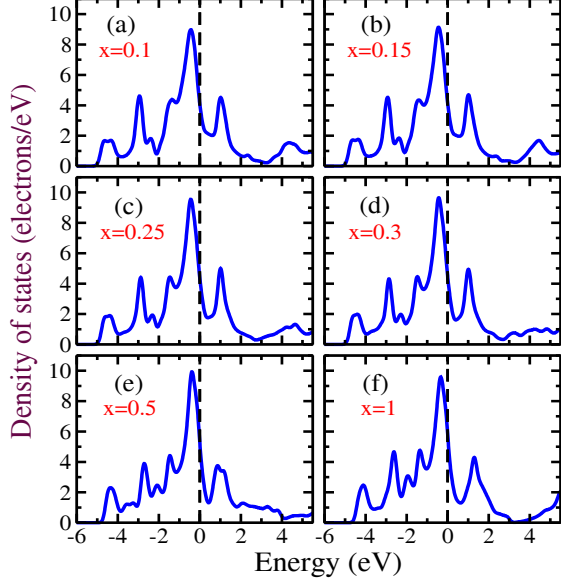


FIG. 4: Calculated atom projected density of states within VCA method for Fe atoms in K doped (hole doping) Ba122 system ($\text{Ba}_{1-x}\text{K}_x\text{Fe}_2\text{As}_2$) in the orthorhombic phase for various doping concentrations, indicated in the figure.

BaFe_2As_2 system are also considered in our investigation. In the theoretical method section we have already described the method of calculation of Stoner factor of a compound system within density functional theory. Virtual crystal approximation (VCA) and super-cell methods are used to mimic various doped 122 Fe-based superconducting systems. We employed experimental lattice parameters a , b , c and z_{As} in both the orthorhombic and tetragonal phases for our first principles electronic structure (DOS and FSs) calculations. It is well known that in 122 Fe-based SCs, DOS at the Fermi level is dominated by Fe-d orbital and to some extent by As-p orbitals. It is for this reason, the particular case of doping at the Fe site is treated within super-cell method in order to calculate the atom projected DOS for Fe and Co/Ru atoms separately with desirable precision. It should be mentioned here that within VCA method, the atom projected DOS of Fe and Ru/Co atoms can not be estimated separately. And for other doping cases (K/Na doping at the Ba site and P doping at As site) we employ VCA for implementation of doping (in which Fe atom projected DOS can be obtained). We have also employed super-cell method for implementing K/Na/P doping in 122 system, but the results of which are not presented here, are very similar to that of the VCA results. First, we calculate the atom projected DOS for Co doped Ba122 systems (electron doping) for several Co doping concentrations in the tetragonal phase. In FIG.1, DOS contribution of Fe and Co atoms are separately presented for various doping concentrations, indicated in the figures. As discussed earlier, for electron doped system (like Co doping at Fe site) superconducting as well as other exotic

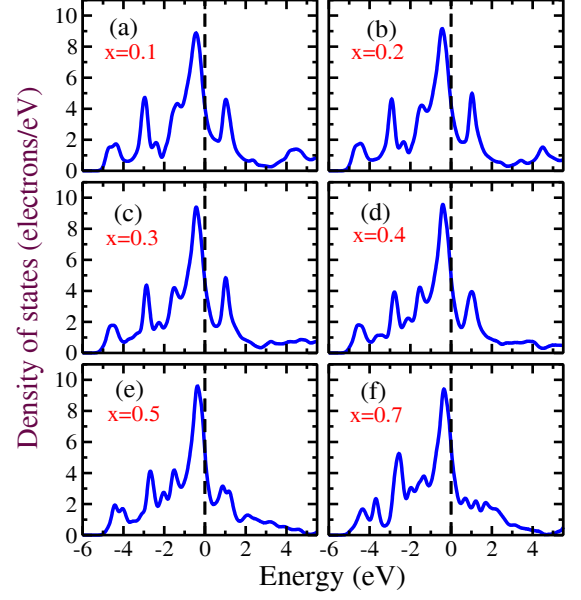


FIG. 5: Calculated atom projected density of states within VCA method for Fe atoms in Na doped (hole doping) Ba122 system ($\text{Ba}_{1-x}\text{Na}_x\text{Fe}_2\text{As}_2$) in the orthorhombic phase for various doping concentrations, indicated in the figure.

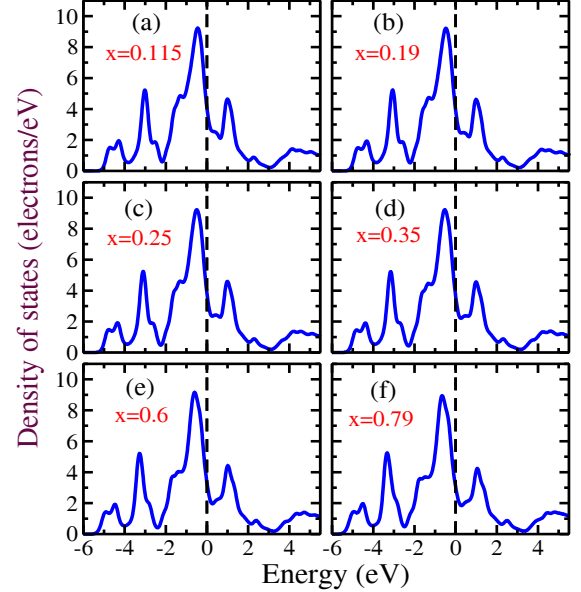


FIG. 6: Calculated atom projected density of states within VCA method for Fe atoms in P doped (iso-electronic doping) Ba122 system $\text{BaFe}_2(\text{As}_{1-x}\text{P}_x)_2$ in the orthorhombic phase for various doping concentrations, indicated in the figure.

phases appear in the system within 10% to 15% doping concentration which is smaller compared to that for other doped 122 systems (for example, superconductivity arises in Ru doped Ba122 system at a very high doping concentration). That is why we restrict our calculation in the low doping regime in the case of Co doped Ba122

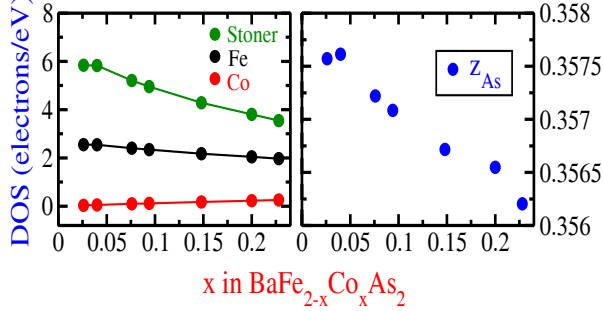


FIG. 7: (a) Contrasting nature of Stoner factor (green) of $\text{BaFe}_{2-x}\text{Co}_x\text{As}_2$ system in the tetragonal phase as a function of Co doping concentration. Variation of density of states of Fe (black) and Co (red) as a function of Co doping concentration is also shown. (b) Variation of experimental (also one of the input parameter of our calculation) z_{As} (fractional z co-ordinate of As atom) with Co doping concentration.

system. We depict atom projected DOS in the tetragonal phase for Ru doped Sr122 and Ba122 systems in FIG.2 and FIG.3 respectively. In those figures, DOS contribution of Ru and Fe atoms are presented separately as a function of Ru doping concentration. In this case our study is no longer restricted to low doping regime but extended our investigation for whole regime of doping concentrations (low to high). On the other hand, we exhibit atom projected DOS in the orthorhombic phase for Fe atom in case of K, Na and P doped Ba122 systems in FIG.4, FIG.5 and FIG.6 respectively. Moreover, atom projected DOS in the tetragonal phase for K, Na and P doped Ba122 systems are also calculated but not presented here. In these cases we employ VCA method for handling doped systems as Fe site is not directly affected by K and Na doping at the Ba site (hole doping) and P doping at the As site (iso-electronic doping). However, we also calculate Fe atom projected DOS for these systems using super-cell approach. We find DOS calculated within super-cell method is qualitatively similar to that using VCA method.

Using this atom projected DOS, we calculate Stoner factor using the method, described in the theoretical method section for various doped 122 systems. In FIG.7a, we display the Stoner factor as well as atom projected DOS of Fe and Co atoms at Fermi level as a function of Co doping concentration in the tetragonal phase. In FIG.7b we provide estimated z_{As} (also use as an input of our first principles calculation) as a function of Co doping concentration. We observe that with increasing Co doping concentration, both the Stoner factor as well as z_{As} decreases. We have also calculated the FSs of Co doped Ba122 system within VCA method. Our calculated FSs also provide a clear indication of more 3D like FSs with higher Co doping concentration. This 3D like FSs work against nesting and results in suppression of magnetic order (SDW). Since Stoner factor is intimately related to magnetic fluctuation or magnetic instability,

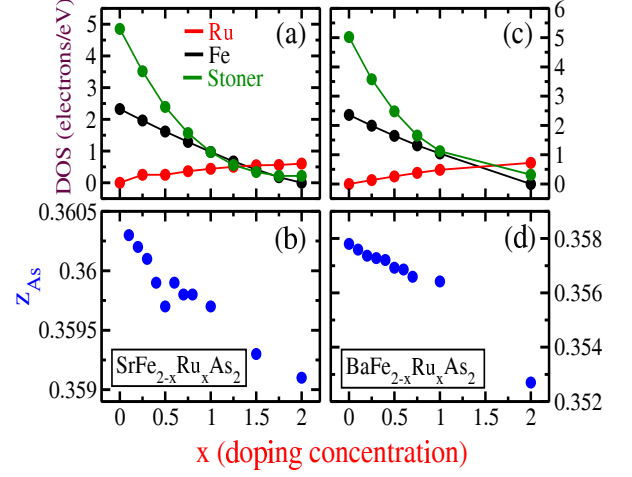


FIG. 8: (a, c) Calculated variation of Stoner factor (green) of $\text{SrFe}_{2-x}\text{Ru}_x\text{As}_2$ and $\text{BaFe}_{2-x}\text{Ru}_x\text{As}_2$ systems in the tetragonal phase as a function of Ru doping concentration respectively. Variation of density of states of Fe (black) and Ru (red) as a function of Ru doping concentration is also shown. (b, d) Variation of experimental (also one of the input parameter of our calculation) z_{As} (fractional z co-ordinate of As atom) with Ru doping concentration.

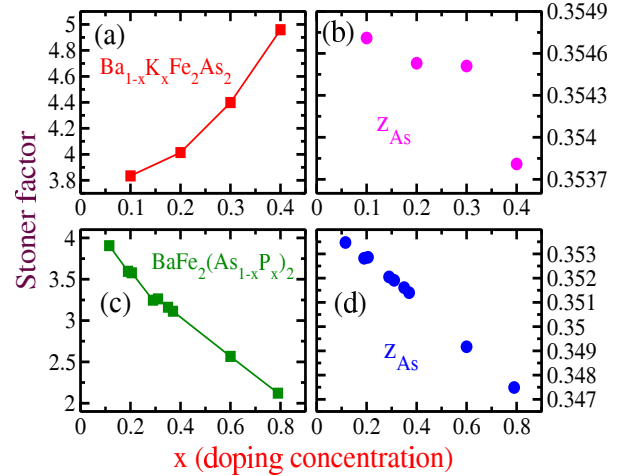


FIG. 9: (a, c) Calculated variation of Stoner factor of $\text{Ba}_{1-x}\text{K}_x\text{Fe}_2\text{As}_2$ and $\text{BaFe}_2(\text{As}_{1-x}\text{P}_x)_2$ systems in the tetragonal phase as a function of K and P doping concentration respectively. (b, d) Variation of experimental z_{As} (also one of the input parameter of our calculation) (fractional z co-ordinate of As atom) with doping concentration.

reduction of Stoner factor with increasing Co doping concentration gives a clear indication of depletion of possible “magnetic fluctuation” in the system with the introduction of Co. This is consistent with the evolution of calculated FSs as a function of doping. Now we move to the case of iso-electronic doping at Fe site (Ru doping at Fe site of Ba122 and Sr122 systems). For both the systems with increasing doping concentration z_{As} decreases

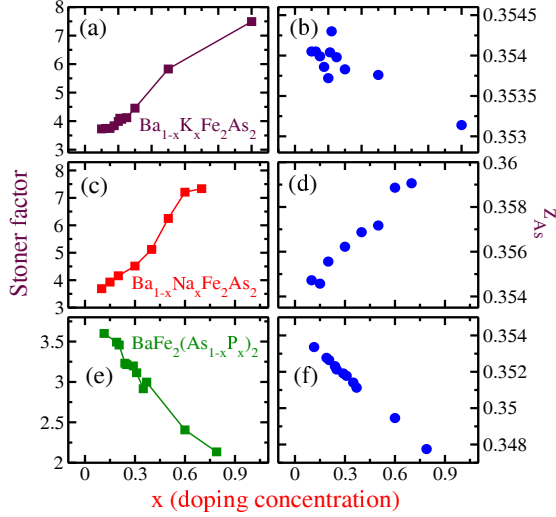


FIG. 10: (a, c, e) Calculated variation of Stoner factor of $Ba_{1-x}K_xFe_2As_2$, $Ba_{1-x}Na_xFe_2As_2$ and $BaFe_2(As_{1-x}P_x)_2$ systems in the orthorhombic phase as a function of K, Na and P doping concentration respectively. (b, d, f) Variation of experimental (also one of the input parameter of our calculation) z_{As} (fractional z co-ordinate of As atom) with doping concentration.

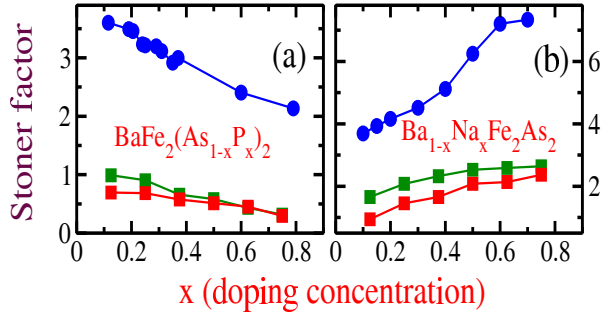


FIG. 11: Calculated variation of Stoner factor of (a) $BaFe_2(As_{1-x}P_x)_2$ and (b) $Ba_{1-x}Na_xFe_2As_2$ systems in the orthorhombic phase as a function doping concentration for different U values. Blue circles are calculated Stoner factor with $U=0$. Green and red square are the calculated Stoner factor for $U=0.5$ and $U=1$ respectively.

as shown in FIG.8b and FIG.8d. In FIG.8a and FIG.8c atom projected DOS at the Fermi level for Ru and Fe atoms as well as Stoner factor are shown as a function of Ru doping concentration for tetragonal Sr122 and Ba122 systems respectively. For both the cases Stoner factor decreases with increasing Ru doping concentration in a very similar manner. We have also performed the FS calculation for Ru doped Sr122 system within supercell method for 50% Ru doping case. We find that for 122 system 50% Ru doping modifies the FSs from 2D like to more 3D like, which is consistent with previous theoretical and experimental investigations [53, 54]. This in-turn degrades the nesting of FSs and triggers superconductiv-

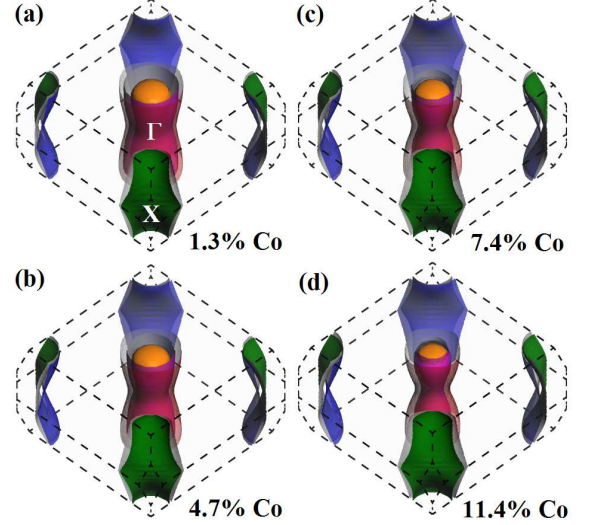


FIG. 12: Calculated FSs of various Co doped Ba122 systems. Doping concentration is also indicated in the figure. Different colours are used to indicate different FSs. There are three hole like FSs around Γ point (centre of the BZ) and two electron like FSs around X point (four corners of the BZ). With increasing doping concentration hole like FSs shrink and electron like FSs expand (electron doping). Also for higher doping concentrations the FSs are more 3D like.

ity in the systems by means of suppression of SDW order or magnetic order. This again creates an impression of curtailment of magnetic order with increasing Ru doping concentration, which is also consistent with the calculated variation of Stoner factor with Ru doping. As far as our FS calculation is concerned, upto 50% Ru doping in Sr122 system, no significant moderation is observed in the FS topology in contrast to Ba122 system. However $SrRu_2As_2$ has completely 3D like FSs just like $BaRu_2As_2$ system, presented in FIG.13c. In FIG.13d we depict the calculated FSs of 50% Ru doped Sr122 system within VCA method. The topology of FSs calculated within VCA method, certainly do not match with the experimental one as reported in literature [53].

Next we calculate the evolution of Stoner factor for K, Na and P doped Ba122 system with increasing doping concentration. In FIG.9a, c the variation of Stoner factor as a function of doping concentration has been shown for K and P doped tetragonal Ba122 systems respectively. In FIG.9b, 9f the variation of z_{As} with doping concentration is also presented for the above mentioned systems respectively. Calculated evaluation of Stoner factors in the orthorhombic Ba122 systems also show similar trends as that of the tetragonal K, Na and P doped Ba122 systems, shown in FIG.10. In FIG.10b and 10f, the variation of z_{As} with doping concentration is also presented for the same systems respectively. In case of K and Na doped systems (hole doped) Stoner factor increases with the increase of doping concentration which also corroborates well with

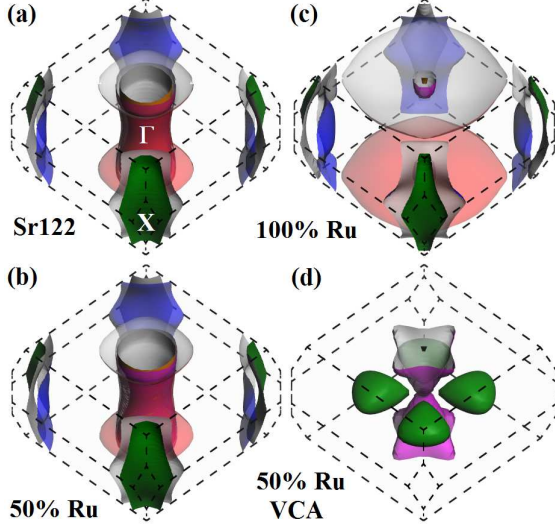


FIG. 13: Calculated FSs of (a) undoped Sr122 (b) 50% and (c) 100% Ru doped Sr122 system using super-cell method. (d) Calculated FSs of 50% Ru doped Sr122 system within VCA method. Doping concentration is also indicated in the figure. Different colours are used to indicate different FSs. There are three hole like FSs around Γ point (centre of the BZ) and two electron like FSs around X point (four corners of the BZ). With 50% Ru doping there is no significant change in the FS topology but most of the FSs of 100% Ru doped Sr122 system are completely 3D like. Calculated FSs for 50% Ru doped Sr122 system within VCA method, do not matches with experimental observations.

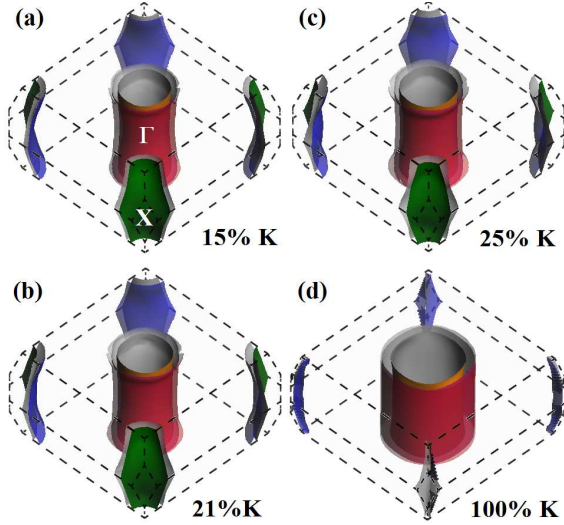


FIG. 14: Calculated FSs of various K doped Ba122 systems. Doping concentration is also indicated in the figure. Different colours are used to indicate different FSs. There are three hole like FSs around Γ point (centre of the BZ) and two electron like FSs around X point (four corners of the BZ). With increasing doping concentration hole like FSs expand and electron like FSs shrink (hole doping). Also for higher doping concentrations the FSs are more 2D like. For 100% K doped system electron like FSs almost disappear.

the nature of the calculated FSs, shown in FIG.14 and 15. Although exactly opposite trends in the behaviour of z_{As} with doping concentration (experimental) is observed in case of K and Na doping (see FIG10b and d) which makes the Na doped system different from other hole doped 122 systems. For P doped system both z_{As} and Stoner factor decreases with increasing doping concentration, which indicate reduction of magnetic instability with P doping. So in general, the Stoner factors of various 122 systems follow the variation of z_{As} with doping except in the case of K doped Ba122 system where the variation of z_{As} with doping is not well defined. Experimental data of z_{As} for K doped Ba122 is not as consistent (probably accurate) compared to that for the other doped 122 family of compounds (see FIG. 10b, d). Since our theoretical calculation is based on the experimental crystallographic data as input, the calculated electronic structure differs from general observation (actually the experimental inconsistency in z_{As} with doping is reflected in the calculated results). In case of $Ba_{1-x}K_xFe_2As_2$, thus, comparison of Stoner factor with z_{As} would not be a correct quantity to look into but the Fe-As bond length as a function of doping concentration. Actually, Stoner factor universally follows the variation of Fe-As bond length for various types of doping. In case of hole doping, Stoner factor inversely follows Fe-As bond length with the variation of doping concentration. On the other hand, in the case of electron doping, Stoner factor follows the doping dependent behaviour of Fe-As bond length. In order to understand universality in the behaviour of Stoner factor and z_{As} /Fe-As bond length of hole doped Ba122, we shed more light into the other structural parameters. To elucidate the inconsistency in the behaviour of Stoner factor and z_{As} in K doped Ba122, we introduce in plane and out of plane As-As distances which also play very important and crucial role. Size of the Ba atom (2.22Å) [atomic radius in metallic bonding] is larger than Na atom (1.86Å) but smaller than K atom (2.27Å). Because of this reason, with the substitution of K atom in place of Ba atom, out of plane As-As distance increases and exactly opposite behaviour in the out of plane As-As distance is observed in the case of Na substitution at Ba site. It should also be noted that the c-axis increases with the increasing doping concentration for both Na and K doping (in case of Na doped Ba122 materials c-axis increases with doping up to certain doping concentration and after that it decreases). This qualitatively explains the observed behaviour of z_{As} with doping for K and Na doped Ba122 systems [55]. But in both the cases Fe-As bond length decreases with increasing doping concentration. Calculated Stoner factors for K/Na/P doped 122 systems using super-cell approach also follow the same trends as that of the calculated one within VCA method. Calculated FSs also become more and more 3D like with increasing P doping concentration, which is consistent with the suppression of magnetic order as observed in experiments (see FIG.16). On the contrary to all other cases of doping, hole doping makes the FSs more 2D like which actually helps having

larger degree of nesting of FSs. This increasing trend of Stoner factor with doping, may be related to the more 2D like FSs of the hole doped 122 systems that enhances nesting segments. In all these 122 systems, superconductivity emerges into the system with certain percentage of doping concentration (small or large). On the contrary to other 122 Fe-based SCs, Stoner factor of hole doped 122 systems (K/Na doped) display distinctly different behaviour. In these cases only, the Stoner factor increases with increasing doping concentration which indicate that, these systems become more and more unstable against magnetic instability. So in these hole doped 122 systems, superconductivity arises at the same moment when magnetic instability also dominates. We have also studied the behaviour of Stoner factor in presence of electron correlation which can be introduced through LDA+U calculation within DFT. Since Fe based SCs specially 122 systems are weakly correlated, we restrict our LDA+U calculation for a small value of U, which defines the strength of correlation ($U=0.5$ and $U=1$). In FIG.11 the variation of Stoner factor with doping concentration for various U values ($U=0.5$ and $U=1$) are depicted for $\text{BaFe}_2(\text{As}_{1-x}\text{P}_x)_2$ and $\text{Ba}_{1-x}\text{Na}_x\text{Fe}_2\text{As}_2$ systems in the orthorhombic phase. It is to be noted here that with the introduction of U, Stoner factor decreases for both the cases but shows very similar trends with doping concentration as that in the case of $U=0$. This study (of LDA+U) has also been extended to all other materials presented in this work. The reduction of Stoner factor with correlation is consistent with the current literature [23]. It should also be noted here that K-doped Ba122 systems have the highest superconducting transition temperature (T_c) among all other Fe-based SCs in ambient condition. This may give some impression that superconductivity in these systems is intimately related to magnetic order and magnetic fluctuations. On the whole, our study provides a clear view about the variation of Stoner factor as a function of doping for all variety of doped 122 Fe-based SCs. We also explain the observed diversities in the behaviour of various doped 122 systems by presenting calculated FSs.

The phase diagram of the iron pnictides reveals that the superconducting transition temperature T_c usually shows a dome-like relation with doping. Should the Stoner factor vary with doping in the fashion as T_c in phase diagrams? One should be aware of the fact that both temperature and doping plays a very important role in any phase diagram. In fact in phase diagram, both temperature and doping dependencies of various phases like spin density wave, superconducting phase *etc.*, are known for various Fe based superconductors. However, in our first principles electronic structure calculations, we use experimentally measured doping dependent lattice parameters (a , b , c , z_{As}) at a fixed temperature as input. That is why our calculated Stoner factor does not contain any temperature dependencies (only doping dependency). In general, z_{As} (as well as other structural parameters) has a very sensitive temperature dependen-

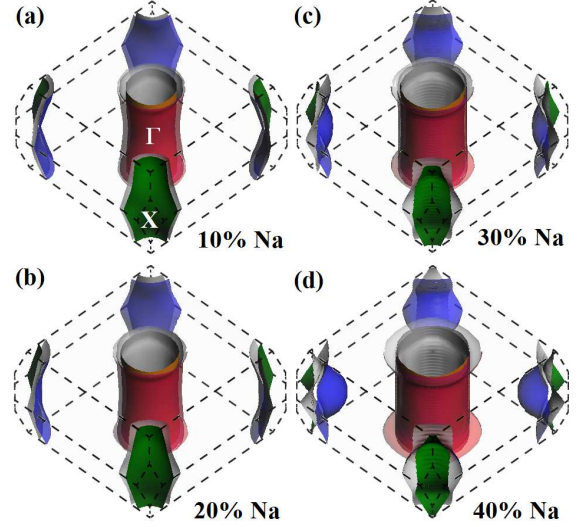


FIG. 15: Calculated FSs of various Na doped Ba122 systems. Doping concentration is also indicated in the figure. Different colours are used to indicate different FSs. There are three hole like FSs around Γ point (centre of the BZ) and two electron like FSs around X point (four corners of the BZ). With increasing doping concentration hole like FSs expand and electron like FSs shrink (hole doping). Also for higher doping concentrations the FSs are more 2D like.

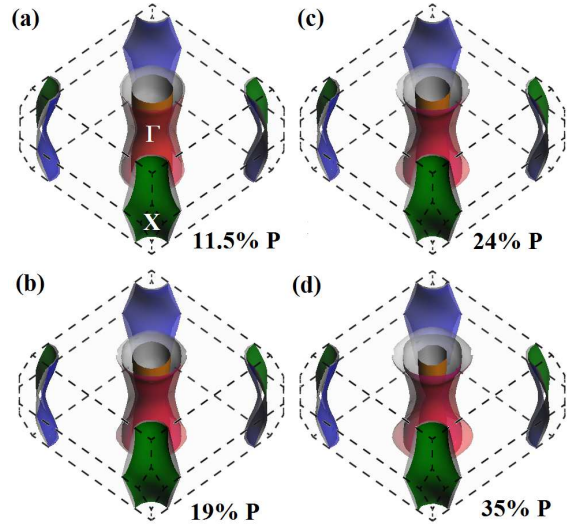


FIG. 16: Calculated FSs of various P doped Ba122 systems. Doping concentration is also indicated in the figure. Different colours are used to indicate different FSs. There are three hole like FSs around Γ point (centre of the BZ) and two electron like FSs around X point (four corners of the BZ). With increasing doping concentration the FSs are more 3D like.

cies. For example, in our earlier work we have shown in Ru doped Ba122 system, structural parameters including z_{As} are highly sensitive to temperature [22]. When such a temperature dependency was included in the electronic structure calculation by us in the past, the temperature dependency of Stoner factor did reproduce the experi-

mental magnetic fluctuation behaviour [32, 56]. In the current perspective where we discuss detailed behaviour of Stoner factor over a wide doping ranges for a number of doped-122 family, clean crystallographic data, particularly z_{As} as a function of both, doping and temperature is not available. As a result such a calculation of Stoner factor as a function doping as well as temperature is only a future possibility. That is why the Stoner factor does not show dome like behaviour.

IV. CONCLUSION

It is well documented that the magnetic fluctuation plays a significant role in superconductivity of Fe-based SCs. Stoner factor is the precursor of magnetic fluctuation or magnetic instability in a system. We have presented in detail the modification of Stoner factor with doping concentration for various doped 122 Fe-based SCs. VCA as well as super-cell methods are employed to dope these materials theoretically to calculate DOS and FSs of doped 122 compounds. Diversities in the behaviour of Stoner factor with varying doping concentrations for various nature of doped 122 systems are discussed. In case of Ru (iso-electronic)/Co (electron) doped systems, Stoner factor decreases with increasing Ru/Co concentration which is compatible with the calculated FSs. Same trends in the behaviour of Stoner factor and FSs are also observed in the case of other iso-electronic doping, P doping at the As site. On the

other hand, in case of hole doped systems (Na/K doping at the Ba site) Stoner factor increases with increasing doping concentration which is also consistent with the corresponding modifications in the calculated FSs for various doping concentrations. Remarkably, we find that the Stoner factor follows the variation as that of the z_{As} with doping. Larger the pnictide height larger is the Stoner factor as well as larger degree of the Fermi surface nesting, larger the value of Stoner factor and vice versa. Sensitive dependence of superconducting T_c with anion height was established earlier [27] but our present work clearly establishes the same for Stoner factor or magnetic fluctuation. As a whole this work provide a comprehensive study of Stoner factor (magnetic instability) for various doped 122 Fe-based SCs.

Acknowledgements

We thank Dr. A. Bharathi and Dr. A. K. Sinha for discussion on experimental aspects. We thank Dr. P. A. Naik and Dr. P. D. Gupta for their encouragement in this work. One of us (SS) acknowledges the HBNI, RRCAT for financial support and encouragements.

Additional information

Competing financial interests: The authors declare no competing financial interests.

-
- [1] G. R. Stewart, Superconductivity in Iron Compounds, Rev. Mod. Phys. 83 (2011), 1589-1641.
 - [2] H. Hosono *et al.*, Exploration of new superconductors and functional materials, and fabrication of superconducting tapes and wires of iron pnictides, Sci. Technol. Adv. Mater. 16 (2015), 033503-033589.
 - [3] R. M. Fernandes, A. V. Chubukov, J. Schmalian, What drives nematic order in iron-based superconductors?, Nature Phys. 10 (2014), 97-104.
 - [4] J. J. Wu *et al.*, Pressure-decoupled magnetic and structural transitions of the parent compound of iron-based 122 superconductors $BaFe_2As_2$, Proc. Natl. Acad. Sci. USA 110 (2013), 17263-17266.
 - [5] H. Kontani, S. Onari, Orbital-Fluctuation-Mediated Superconductivity in Iron Pnictides: Analysis of the Five-Orbital Hubbard-Holstein Model, Phys. Rev. Lett. 104 (2010), 157001-157004.
 - [6] I. I. Mazin, D. J. Singh, M. D. Johannes, M. H. Du, Unconventional Superconductivity with a Sign Reversal in the Order Parameter of $LaFeAsO_{1-x}F_x$ Phys. Rev. Lett. 101 (2008), 057003-057007.
 - [7] A. V. Chubukov, Pairing mechanism in Fe-based superconductors, Annul. Rev. Cond. Mat. Phys. 3 (2012), 13.1.
 - [8] Smritijit Sen and Haranath Ghosh, Intra-inter band pairing, order parameter symmetry in Fe-based superconductors: A model study, J. Alloys Compd. 618 (2015), 102 - 109.
 - [9] S. Avci, O. Chmaissem, D. Y. Chung, S. Rosenkranz, E. A. Goremychkin, J. P. Castellan, I. S. Todorov, J. A. Schlueter, H. Claus, A. Daoud-Aladine, D. D. Khalyavin, M. G. Kanatzidis and R. Osborn, Phase diagram of $Ba_{1-x}K_xFe_2As_2$, Phys. Rev. B, 85 (2012), 184507 - 184519.
 - [10] H. Ghosh and S. Sen, Role of Sn impurity on electronic topological transitions in 122 Fe-based superconductors J. Alloys Compd. 677 (2016) 245-251
 - [11] A. Lucarelli, A. Dusza, F. Pfner, P. Lerch, J. G. Analytis, J.-H. Chu, I. R. Fisher and L. Degiorgi, Charge dynamics of Co-doped $BaFe_2As_2$ New J. Phys. 12 (2010), 073036.
 - [12] X. F. Wang, T. Wu, G. Wu, R. H. Liu, H. Chen, Y. L. Xie and X. H. Chen, The peculiar physical properties and phase diagram of $BaFe_{2-x}Co_xAs_2$ single crystals, New J. Phys., 11 (2009), 045003 - 045014.
 - [13] N. Ni, A. Thaler, A. Kracher, J. Q. Yan, S. L. Bud'ko and P. C. Canfield, Phase diagrams of $Ba(Fe_{1-x}M_x)_2As_2$ single crystals (M=Rh and Pd), Phys. Rev. B, 80 (2009), 024511 - 024518.
 - [14] A. Thaler, N. Ni, A. Kracher, J. Q. Yan, S. L. Bud'ko and P. C. Canfield, Physical and magnetic properties of $Ba(Fe_{1-x}Ru_x)_2As_2$ single crystals Phys. Rev. B 82 (2010), 014534 - 014541.

- [15] S. Nandi, M.G. Kim, A. Kreyssig, R.M. Fernandes, D.K. Pratt, A. Thaler, N. Ni, S.L. Bud'ko, P.C. Canfield, J. Schmalian, R.J. McQueeney, A.I. Goldman, Anomalous Suppression of the Orthorhombic Lattice Distortion in Superconducting $\text{Ba}(\text{Fe}_{1-x}\text{Co}_x)_2\text{As}_2$ Single Crystals, *Phys. Rev. Lett.* 104 (2010), 057006 - 057011.
- [16] S. Kasahara, T. Shibauchi, K. Hashimoto, K. Ikada, S. Tonegawa, R. Okazaki, H. Shishido, H. Ikeda, H. Takeya, K. Hirata, T. Terashima and Y. Matsuda, Evolution from non-Fermi- to Fermi-liquid transport via isovalent doping in $\text{BaFe}_2(\text{As}_{1-x}\text{P}_x)_2$ superconductors, *Phys. Rev. B* 81 (2010), 184519.
- [17] A. Mani, N. Ghosh, S. Paulraj, A. Bharathi and C. S. Sundar, Pressure-induced superconductivity in BaFe_2As_2 single crystal, *Europhys. Lett.* 87 (2009), 17004.
- [18] Tuson Park, Eunsung Park, Hanoh Lee, T. Klimczuk, E. D. Bauer, F. Ronning and J. D. Thompson, Pressure-induced superconductivity in CaFe_2As_2 , *J. Phys.: Condens. Matter* 20 (2008), 322204.
- [19] A. S. Sefat, R. Jin, M. A. McGuire, B. C. Sales, D. J. Singh and D. Mandrus, Superconductivity at 22 K in Co-Doped BaFe_2As_2 Crystals *Phys. Rev. Lett.* 101 (2008), 117004.
- [20] Smritijit Sen, Haranath Ghosh, A. K. Sinha, A. Bharathi, Origin of structural and magnetic transitions in $\text{BaFe}_{2-x}\text{Ru}_x\text{As}_2$ materials, *Supercond. Sci. Technol. (Fast Track Communication)* 27 (2014), 122003-122009.
- [21] Deepa Kasinathan, Alim Ormeci, Katrin Koch, Ulrich Burkhardt, Walter Schnelle, Andreas Leithe-Jasper and Helge Rosner, *New J. Phys.*, 11 (2009), 025023.
- [22] S. Sharma, A. Bharathi, K. Vinod, C. S. Sundar, V. Srihari, Smritijit Sen, Haranath Ghosh, Anil K. Sinha and S. K. Deb, Structural investigations in $\text{BaFe}_{2-x}\text{Ru}_x\text{As}_2$ as a function of Ru and temperature *Acta Cryst. B* 71 (2015), 61-67.
- [23] I. I. Mazin and D. J. Singh, Electronic structure and magnetism in Ru-based perovskites, *Phys. Rev B* 56 (1997), 2556.
- [24] Shilpam Sharma, A. Bharathi, Sharat Chandra, Raghavendra Reddy, S. Paulraj, A. T. Satya, V. S. Sastri, Ajay Gupta, C. S. Sundar, Superconductivity in Ru-substituted polycrystalline $\text{BaFe}_{2-x}\text{Ru}_x\text{As}_2$, *Phys. Rev B* 81 (2010), 174512.
- [25] F. Han, X. Zhu, P. Cheng, G. Mu, Y. Jia, L. Fang, Y. Wang, H. Luo, B. Zeng, B. Shen, L. Shan, C. Ren and H.-H. Wen, Superconductivity and phase diagrams of the 4d- and 5d-metal-doped iron arsenides $\text{SrFe}_{2-x}\text{M}_x\text{As}_2$ ($\text{M}=\text{Rh}, \text{Ir}, \text{Pd}$), *Phys. Rev. B* 80 (2009), 024506.
- [26] S. Avci, *et al.*, Magnetically-Driven Suppression of Nematic Order in an Iron-Based Superconductor, *Nat. Commun.* 5 (2014), 3845-3850.
- [27] Y. Mizuguchi, Y. Hara, K. Deguchi, S. Tsuda, T. Yamaguchi, K. Takeda, H. Kotegawa, H. Tou, Y. Takano, Anion height dependence of T_c for the Fe-based superconductor, *Super. Sci. Tech.*, 23 (2010), 054013.
- [28] A. K. Ganguli, J. Prakash and G. S. Thakur, The iron-age of superconductivity: structural correlations and commonalities among the various families having -Fe-Pn-slabs ($\text{Pn} = \text{P}, \text{As}$ and Sb), *Chem. Soc. Rev.* 42 (2013), 569.
- [29] C. H. Lee, K. Kihou, A. Iyo, H. Kito, P. M. Shirage, H. Eisaki, Relationship between crystal structure and superconductivity in iron-based superconductors, *Solid State Commun.* 152 (2012), 644.
- [30] Jun Zhao, Q. Huang, Clarina de la Cruz, Shiliang Li, J. W. Lynn, Y. Chen, M. A. Green, G. F. Chen, G. Li, Z. Li, J. L. Luo, N. L. Wang and Pengcheng Dai, Structural and magnetic phase diagram of CeFeAsO , *Nat Mater.* 12 (2008), 953.
- [31] P. M. Shirage, K. Miyazawa, M. Ishikado, K. Kihou, C. H. Lee, N. Takeshita, H. Matsuhata, R. Kumai, Y. Tomioka, T. Ito, H. Kito, H. Eisaki, S. Shamoto, A. Iyo, High-pressure synthesis and physical properties of new iron (nickel)-based superconductors, *Physica C* 469 (2013), 355.
- [32] Smritijit Sen and Haranath Ghosh, Nematicity, magnetic fluctuation and ferro-spin-orbital ordering in BaFe_2As_2 family, *J. Alloys Compd.* 675 (2016) 416-422.
- [33] H. Luo, *et al.*, Spin Excitation Anisotropy as a Probe of Orbital Ordering in the Paramagnetic Tetragonal Phase of Superconducting $\text{BaFe}_{1.904}\text{Ni}_{0.096}\text{As}_2$, *Phys. Rev. Lett.* 111 (2013), 107006-107011.
- [34] X. Lu, *et al.*, Nematic spin correlations in the tetragonal state of uniaxial-strained $\text{BaFe}_{2-x}\text{Ni}_x\text{As}_2$, *Science* 345 (2014) 657-660.
- [35] A. E. Taylor, M. J. Pitcher, R. A. Ewings, T. G. Perring, S. J. Clarke and A. T. Boothroyd, Antiferromagnetic spin fluctuations in LiFeAs observed by neutron scattering, *Phys. Rev. B* 83 (2011), 220514(R).
- [36] L. Ortenzi, I. I. Mazin, P. Blaha and L. Boeri, Accounting for spin fluctuations beyond local spin density approximation in the density functional theory, *Phys. Rev. B* 86 (2012), 064437.
- [37] J. Ferber, Y.-Z. Zhang, H. O. Jeschke, and R. Valentí, Analysis of spin-density wave conductivity spectra of iron pnictides in the framework of density functional theory, *Phys. Rev. B* 82 (2010), 165102.
- [38] S. J. Clark, *et al.*, First principles methods using CASTEP, *Zeitschrift fuer Kristallographie* 220 (2005), 567-570.
- [39] J. P. Perdew, K. Burke, M. Ernzerhof, Generalized Gradient Approximation Made Simple, *Phys. Rev. Lett.* 77 (1996), 3865-3868.
- [40] D. J. Singh, Electronic structure and doping in BaFe_2As_2 and LiFeAs : Density functional calculations, *Phys. Rev. B* 78 (2008), 094511.
- [41] L. Zhang and D. J. Singh, Electronic structure of $\text{Ba}(\text{Fe}, \text{Ru})_2\text{As}_2$ and $\text{Sr}(\text{Fe}, \text{Ir})_2\text{As}_2$ alloys, *Phys. Rev. B* 79 (2009), 174530.
- [42] Z. P. Yin, S. Lebegue, M. J. Han, B. P. Neal, S. Y. Savrasov, W. E. Pickett, Electron-Hole Symmetry and Magnetic Coupling in Antiferromagnetic LaFeAsO , *Phys. Rev. Lett.* 101 (2008), 047001.
- [43] I. I. Mazin, Problems with reconciling density functional theory calculations with experiment in ferropnictides, *Phys. Rev. B* 78 (2008), 085104.
- [44] M. Rotter, High-temperature superconductivity in doped BaFe_2As_2 , PhD thesis, Ludwig-Maximilians-Universität München, (2010) p. 61.
- [45] S. Avci, *et al.*, Structural, magnetic, and superconducting properties of $\text{Ba}_{1-x}\text{Na}_x\text{Fe}_2\text{As}_2$ *Phys. Rev. B* 88 (2013), 094510.
- [46] J. M. Allred *et al.*, Coincident structural and magnetic order in $\text{BaFe}_2(\text{As}_{1-x}\text{P}_x)_2$ revealed by high-resolution neutron diffraction *Phys. Rev. B* 90 (2014), 104513.
- [47] L. Bellaiche and D. Vanderbilt, Virtual crystal approx-

- imation revisited: Application to dielectric and piezoelectric properties of perovskites, Phys. Rev.B 61 (2000), 7877.
- [48] Smritijit Sen and Haranath Ghosh, Electronic structures of doped BaFe_2As_2 materials: virtual crystal approximation versus super-cell approach, Eur. Phys. J. B 89 (2016), 277.
 - [49] P. Dai *et al.*, Magnetism and its microscopic origin in iron-based high-temperature superconductors, Nature, 8 (2012) 709.
 - [50] O. K. Andersen, J. Madsen, U. K. Poulsen, O. Jepsen, J. Kollár, Magnetic ground state properties of transition metals, Physica C 86-88 (1977), 249-256; E. C. Stoner, Proceedings of the Royal Society A: Mathematical, Physical and Engineering Sciences 165 (1938), 372-414.
 - [51] J. Q. Yan, *et al.*, Structural transition and anisotropic properties of single-crystalline SrFe_2As_2 Phys. Rev. B 78 (2008), 024516-024519.
 - [52] A. S. Sefat, D. J. Singh *et al.*, Renormalized behavior and proximity of BaCo_2As_2 to a magnetic quantum critical point Phys. Rev.B 79 (2009), 024512-024517.
 - [53] Smritijit Sen, Haranath Ghosh, Fermiology of 122 family of Fe-based superconductors: An ab initio study Phys. Lett. A 379 (2015), 843 -847.
 - [54] N. Xu, T. Qian, P. Richard, Y.-B. Shi, X.-P. Wang, P. Zhang, Y.-B. Huang, Y.-M. Xu, H. Miao, G. Xu, G.-F. Xuan, W.-H. Jiao, Z.-A. Xu, G.-H. Cao, H. Ding, Effects of Ru substitution on electron correlations and Fermi-surface dimensionality in $\text{Ba}(\text{Fe}_{1-x}\text{Ru}_x)_2\text{As}_2$, Phys. Rev. B 86 (2012), 064505 - 064509.
 - [55] Haranath Ghosh, Smritijit Sen and Abyay Ghosh, Journal of Physics and Chemistry of Solids 102 (2017), 157167.
 - [56] K. Matan, R. Morinaga, K. Iida, and T. J. Sato, Anisotropic itinerant magnetism and spin fluctuations in BaFe_2As_2 : A neutron scattering study, Phys. Rev. B 79 (2009), 054526.